

Article

Method for Ranking Pulse-like Ground Motions According to Damage Potential for Reinforced Concrete Frame Structures

Qinghui Lai ^{1,2} , Jinjun Hu ^{3,*} , Longjun Xu ^{1,2}, Lili Xie ^{1,2,3} and Shibin Lin ^{1,2}

¹ State Key Laboratory of Precision Blasting, Jiangnan University, Wuhan 430056, China; laiqinghui@jhun.edu.cn (Q.L.); xulj@jhun.edu.cn (L.X.); 18845117968@163.com (L.X.); shibinlin@gmail.com (S.L.)

² Hubei Key Laboratory of Blasting Engineering, Jiangnan University, Wuhan 430056, China

³ Key Laboratory of Earthquake Engineering and Engineering Vibration, Institute of Engineering Mechanics, China Earthquake Administration, Harbin 150080, China

* Correspondence: hujinjun@iem.ac.cn

Abstract: To rank the pulse-like ground motions based on the damage potential to different structures, the internal relationship between the damage potential of pulse-like ground motions and engineering demand parameters (*EDPs*) is analyzed in this paper. First, a total of 240 pulse-like ground motions from the NGA-West2 database and 16 intensity measures (*IMs*) are selected. Moreover, four reinforced concrete frame structures with significantly different natural vibration periods are established for dynamic analysis. Second, the efficiency and sufficiency of the *IMs* of ground motion are analyzed, and the *IMs* that can be used to efficiently and sufficiently evaluate the *EDPs* are obtained. Then, based on the calculation results, the principal component analysis (*PCA*) method is employed to obtain a comprehensive *IM* for characterizing the damage potential of pulse-like ground motions for specific building structures and *EDPs*. Finally, the pulse-like ground motions are ranked based on the selected *IM* and the comprehensive *IM* for four structures and three *EDPs*. The results imply that the proposed method can be used to efficiently and sufficiently characterize the damage potential of pulse-like ground motions for building structures.

Keywords: pulse-like ground motions; damage potential ranking; intensity measures; analysis of efficiency and sufficiency; principal component analysis



Citation: Lai, Q.; Hu, J.; Xu, L.; Xie, L.; Lin, S. Method for Ranking Pulse-like Ground Motions According to Damage Potential for Reinforced Concrete Frame Structures. *Buildings* **2022**, *12*, 754. <https://doi.org/10.3390/buildings12060754>

Academic Editor: Eva O. L. Lantsoght

Received: 10 April 2022

Accepted: 22 April 2022

Published: 1 June 2022

Publisher's Note: MDPI stays neutral with regard to jurisdictional claims in published maps and institutional affiliations.



Copyright: © 2022 by the authors. Licensee MDPI, Basel, Switzerland. This article is an open access article distributed under the terms and conditions of the Creative Commons Attribution (CC BY) license (<https://creativecommons.org/licenses/by/4.0/>).

1. Introduction

Ground motion damage to building structures is of two types: (1) cumulative damage, which occurs due to ground motion at medium and faraway sites; (2) instantaneous damage, which primarily occurs due to the destructive pulse-like ground motion. The mechanisms of the two types of ground motion damage are different. The damage potential of pulse-like ground motions for building structures is more significant compared with that of ordinary ground motions [1–4]. Therefore, the damage potential of pulse-like ground motions must be accurately evaluated for the seismic design of building structures. To estimate the damage potential of ground motions for building structures, two intermediate variables are introduced—one represents structural performance and the other represents ground motion characteristics [5–8]. An intensity measure (*IM*) that has a strong correlation with the appropriate engineering demand parameter (*EDP*) must be selected. However, several *IMs* can be used to predict structural responses by establishing a seismic demand model between *IMs* and *EDPs* [3,9,10]. Yazdani and Yazdannejad [11] noted that the uncertainties associated with the seismic demand model are related to uncertainties associated with ground motions.

A few studies have focused on commonly used *IMs* such as peak ground acceleration (*PGA*), peak ground velocity (*PGV*), peak ground displacement (*PGD*), Arias intensity (*AI*), specific energy density (*SED*), and cumulative absolute velocity (*CAV*) [12]. However,

these *IMs* are based only on ground motion characteristics, and the uncertainties associated with structural performance are not considered. The more ground motion information and structural information an *IM* contains, the better the correlation with *EDPs* is. Compared with the aforementioned *IMs*, the first-order spectral acceleration ($S_a(T_1)$) is the most extensively used *IM* in seismic risk analysis and structural seismic analysis [13–19]. $S_a(T_1)$ presents a high degree of correlation with the *EDPs* of structures with small natural vibration periods. However, several studies [20,21] have discovered that there is a low degree of correlation between the $S_a(T_1)$ and *EDPs* of super-high-rise buildings. To this end, some experts have selected relative displacement ($S_d(T_1)$) or input energy ($E_i(T_1)$) as the *IMs* for predicting structural responses [18,22]. A few studies have focused on achieving discreteness in vector *IMs* and *EDPs* [23,24]; the discreteness achieved in vector *IMs* and *EDPs* is smaller than that in scalar *IMs*. However, vector *IMs* are complex and thus not conducive to practical engineering applications. To avoid the complexities associated with the use of vector *IMs*, scalar *IMs* can be used instead, especially when the same capacity for predicting *EDPs* can be achieved using scalar *IMs* [25,26].

Significant uncertainties are prevalently associated with structural performance. However, in some studies, only a few similar structures have been comprehensively analyzed via non-linear time-history analysis [9,20,26,27]; the results obtained in this direction are consistent. Ebrahimian [9] analyzed the prediction capacities of different *IMs* for the structural responses of four-story and six-story isolated structures, which were subjected to pulse-like ground motions and ordinary ground motion. The results implied that the vector *IMs* related to $S_a(T_1)$ could be used to predict structural responses more efficiently and sufficiently. Dávalos and Miranda [26] analyzed the efficiency and sufficiency of *FIV3* in predicting the structural responses of a four-story reinforced concrete (RC) frame. The results indicated that the novel *FIV3* is a promising parameter that can be used for assessing structural collapse risks. Furthermore, some researchers have investigated the correlation between the *IMs* and structural responses of different structures. Palanci [28] analyzed the correlation between the average values of spectral displacement over different periods via the SDOF system involving different hysteretic models. However, in this study, the correlation between different *IMs* and the average values of *EDPs* of different structures is investigated to determine the prediction capacities of *IMs*, without considering the uncertainties associated with the structures. Note that the correlations between the *EDPs* and different *IMs* are significantly different for structures with different natural vibration periods [29–31]. Yakhachalian and Ghodrati [29] analyzed the discreteness of *IMs* and *EDPs* for low- and middle-rise structures via the strip method. The vector *IM* ($S_a(T_1)$, $S_d(T_1)/PGV$) is proposed as an optimal *IM* for predicting the maximum inter-story drift ratio (*MIDR*) for low- and middle-rise RC moment-resisting frame structures.

However, the aforementioned studies have only verified the prediction capacity of the selected *IMs* for different structures; meanwhile, few studies have used the obtained *IMs* to further analyze ground motion characteristics. The damage potential of ground motions for building structures can be determined based on different *IMs*. Notably, ground motions, especially pulse-like ground motions, have not been ranked based on the optimal *IMs* in the aforementioned studies. In this study, pulse-like ground motions are ranked based on their damage potential for different RC frame structures.

2. Technical Framework

To rank the ground motions in predicting *EDPs* based on the damage potential, a method is proposed for ranking pulse-like ground motions according to their damage potential in this study; the method involves predicting *EDPs* based on ground motion *IMs*. The uncertainties associated with both ground motions and building structures are considered in the proposed method. The 16 selected *IMs* include amplitude, spectrum, and duration, which can be used to describe the uncertainties associated with ground motions. Meanwhile, four reinforced concrete (RC) frame structural models with significantly different natural vibration periods are established, and three *EDPs* are considered for

evaluating the uncertainty of the established structures. The efficiency and sufficiency of IMs in predicting $EDPs$ are analyzed to determine the optimal IMs for different structures. Furthermore, for multiple optimal IMs , the pulse-like ground motions are ranked by determining the comprehensive IM via the principal component analysis (PCA) method. Finally, the pulse-like ground motions are ranked according to their damage potential using the selected optimal IM . The technical framework of this paper is illustrated in Figure 1.

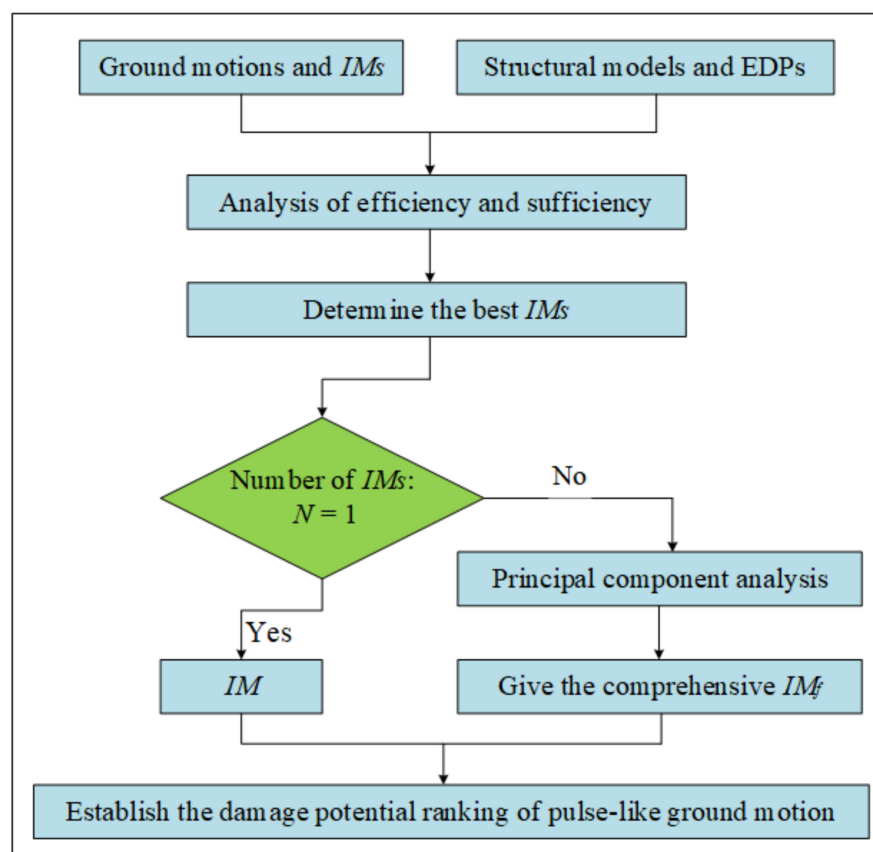


Figure 1. Technical framework.

3. Selection of Pulse-like Ground Motions and IMs

3.1. Selected Pulse-like Ground Motions

Compared with that of ordinary ground motions, the damage potential of pulse-like ground motions is typically higher. Pulse-like ground motions involve the release of significant amounts of instantaneous energy, thereby causing impact damage in building structures. Figure 2 depicts the velocity time-histories of two ground motions, (a) pulse-like ground motion and (b) non-pulse-like ground motion, which are significantly different from each other. In this study, the damage potential of 240 pulse-like ground motions is analyzed; the ground motions are selected according to the method proposed by Zhai [32]. An energy-based significant velocity half-cycle is used as a reference for distinguishing pulse-like ground motions. Note that these pulse-like ground motions are extensively studied [33]. Figure 3 illustrates the station distribution of pulse-like ground motions, which is mainly distributed in the United States, Japan, the Middle East, and Taiwan Province of China. Figure 4 shows the distributions of V_{s30} , magnitude (M), and epicentral distance (R). The values of M range from 5.21 to 7.62, and those of V_{s30} are mainly < 1000 m/s. Pulse-like ground motions can be generated not only in the near field, but also in the relative far field ($R > 100$ km).

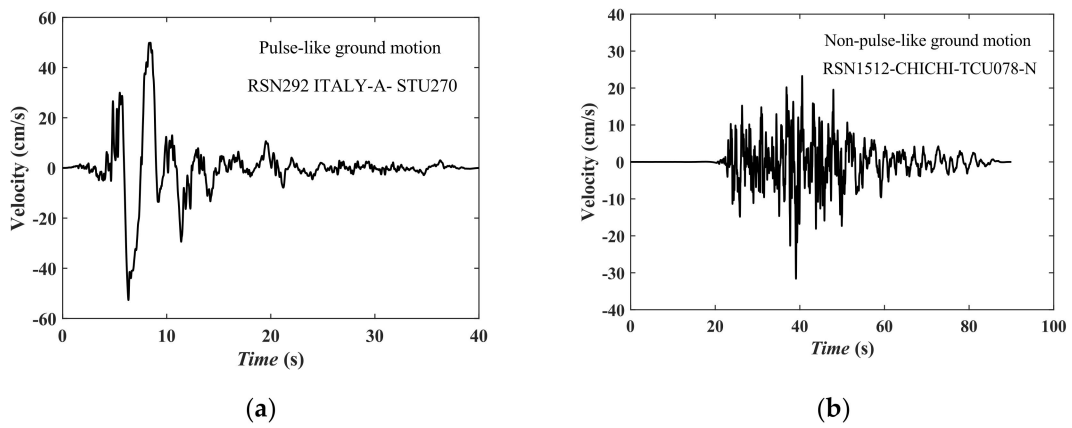


Figure 2. Velocity time-history of pulse-like and non-pulse-like ground motions. (a) Pulse-like ground motion; (b) non-pulse-like ground motion.

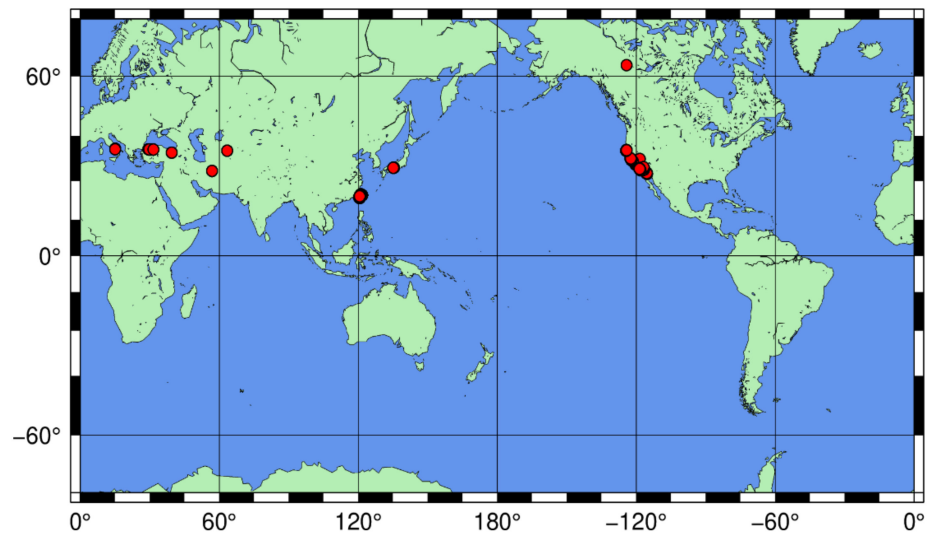


Figure 3. Station distribution of selected pulse-like ground motions.

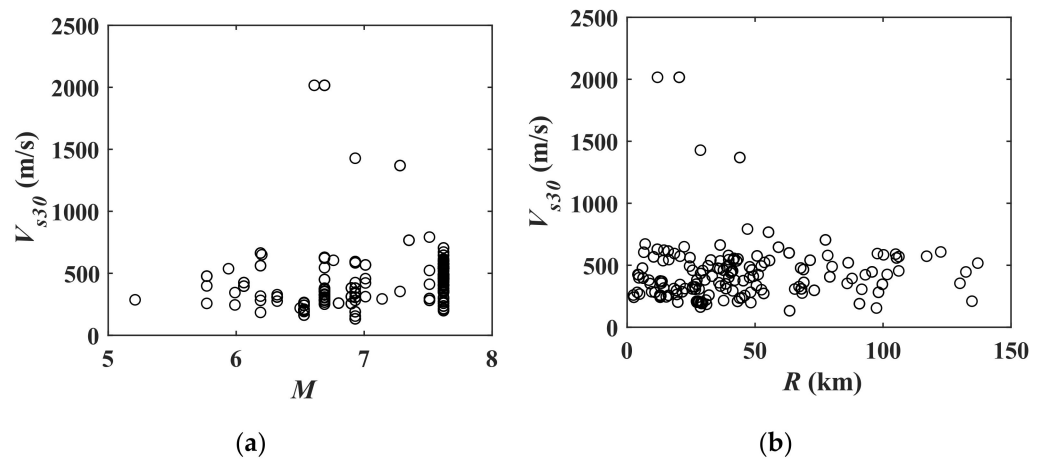


Figure 4. Distribution ranges of M , R , and V_{s30} of the selected pulse-like ground motions. (a) V_{s30} - M ; (b) V_{s30} - R .

3.2. Selected IMs

The main causes of structural damage caused by ground motion are included in the whole ground motion time-history. The time-history characteristics of ground motion are

indicated by various *IMs*. In this study, a novel method is employed for predicting the damage potential of ground motion for building structures; the method involves adopting 16 commonly used *IMs*, including amplitude, duration, spectrum, and energy parameters, based on previous studies. The selected *IMs* are shown in Table 1, and their physical significance and calculation methods are mentioned in the relevant literature [32,34,35].

Table 1. Selected *IMs*.

Note	Ground Motion <i>IMs</i>	Expression
<i>IM</i> ₁	Peak ground acceleration (<i>PGA</i>)	$PGA = \max a(t) $
<i>IM</i> ₂	Peak ground velocity (<i>PGV</i>)	$PGV = \max v(t) $
<i>IM</i> ₃	Peak ground displacement (<i>PGD</i>)	$PGD = \max d(t) $
<i>IM</i> ₄	Bracketed duration (<i>D_b</i>)	$D_b = \max(t) - \min(t)$
<i>IM</i> ₅	Uniform duration (<i>D_u</i>)	$D_u = \int_0^\infty H(a(t) - a_0)dt$
<i>IM</i> ₆	Significant duration (<i>D_s</i>)	$D_s = t_{95} - t_5$
<i>IM</i> ₇	Effective peak acceleration (<i>EPA</i>)	$EPA = S_a/2.5$
<i>IM</i> ₈	Effective peak velocity (<i>EPV</i>)	$EPV = S_v/2.5$
<i>IM</i> ₉	Housner intensity (<i>SI</i>)	$SI_\zeta = \int_{0.1}^{2.5} S_v(\zeta, T)dT$
<i>IM</i> ₁₀	Cumulative absolute velocity (<i>CAV</i>)	$CAV(t) = \sum_i \int_{t_i}^{t_i+1} W_i A(t) dt$
<i>IM</i> ₁₁	Maximum incremental velocity (<i>MIV</i>)	-
<i>IM</i> ₁₂	Maximum incremental displacement (<i>MID</i>)	-
<i>IM</i> ₁₃	Spectral acceleration at the first mode period of vibration (<i>S_a</i> (<i>T</i> ₁))	-
<i>IM</i> ₁₄	Spectral velocity at the first mode period of vibration (<i>S_v</i> (<i>T</i> ₁))	-
<i>IM</i> ₁₅	Spectral displacement at the first mode period of vibration (<i>S_d</i> (<i>T</i> ₁))	-
<i>IM</i> ₁₆	Relative input energy at the first mode period of vibration <i>E_i</i> (<i>T</i> ₁)	$E(T_1) = \sqrt{-2 \int a_g v dt}$

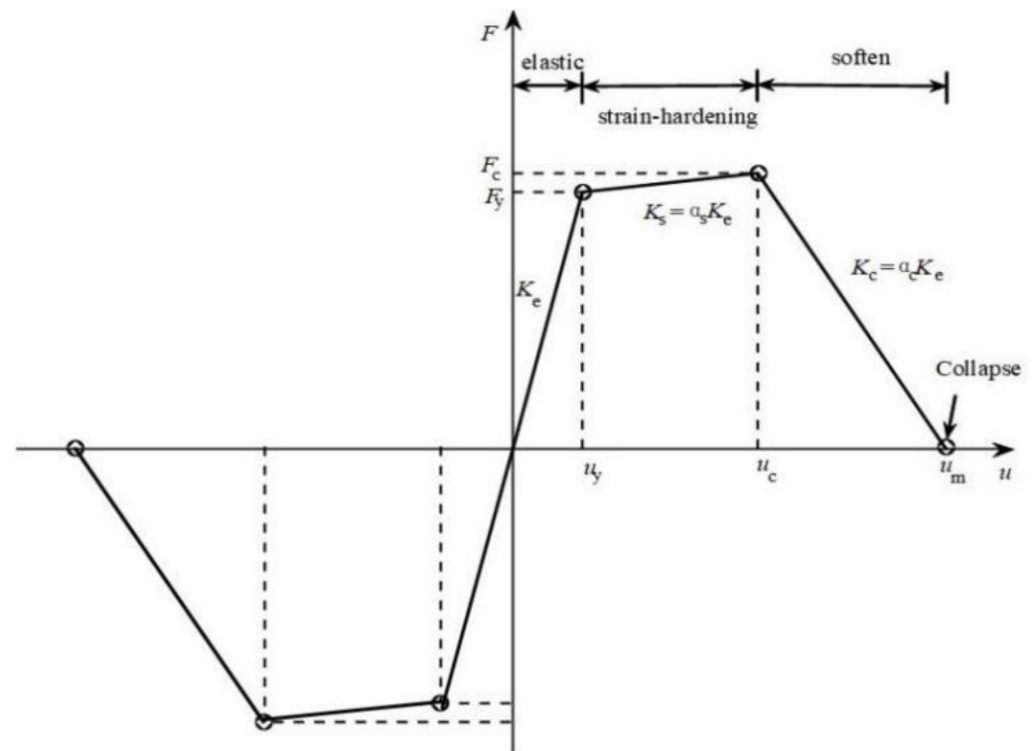
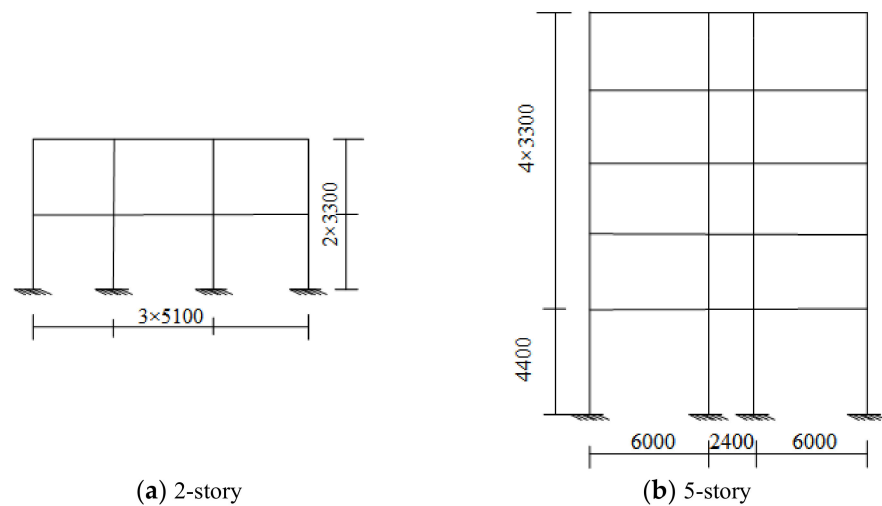
4. Selection of Structural Models and EDPs

4.1. Structural Models

To comprehensively analyze the destruction mechanism of different structures caused by pulse-like ground motions, four representative structural models with quite different natural vibration periods are established and used for comprehensively analyzing the damage caused by pulse-like ground motions in different structures. The structural models are designed according to Zhai et al. [35] and Li et al. [36]. The four frame structures are of different types—short-period, short- and middle-period, middle- and long-period, and long-period—with 2, 5, 8, and 15 stories, respectively. These buildings are symmetric. The finite element software IDARC-2D is used to analyze the four frame structures [37]. The natural vibration period (*T*₁) of each structure is shown in Table 2. The four structural models are based on four ordinary RC frame structures, with seismic fortification intensity of seven degrees. The four structures are modeled considering a class II site. The improved I-K trilinear hysteretic model is used for the four structures [38,39], and Figure 5 shows the hysteretic skeleton curve of the model. The four buildings use C30 concretes, and the live load is 0.4 kN/m². Figure 6 illustrates the plan and elevation of the four representative structures. Tables 3 and 4 show the sectional dimensions, concrete grades, and steel rebars of the beams and columns of the structures. The yielding strength *f_{yk}* of the main reinforcement rebars is 400 MPa, and the yielding strength *f_{yk}* of the stirrups is 300 MPa. During calculations, the stiffness in the floor plane is considered infinite. The stiffness degradation coefficient α , strength degradation coefficient β , and pinch effect coefficient γ determine the hysteretic responses of the structures. The values 8.0, 0.1, and 0.5 are selected for the parameters α , β , and γ , respectively, for the analysis using the IDARC-2D software. Centralized plasticity is considered as the plasticity type.

Table 2. Natural vibration periods and types of structures.

Building Structures	Natural Vibration Period T_1	Structure Types
2-story	0.20 s	Short period
5-story	0.89 s	Short and middle period
8-story	1.73 s	Middle and long period
15-story	2.73 s	Long period

**Figure 5.** Backbone curve for improved I-K hysteretic model.**Figure 6.** Cont.

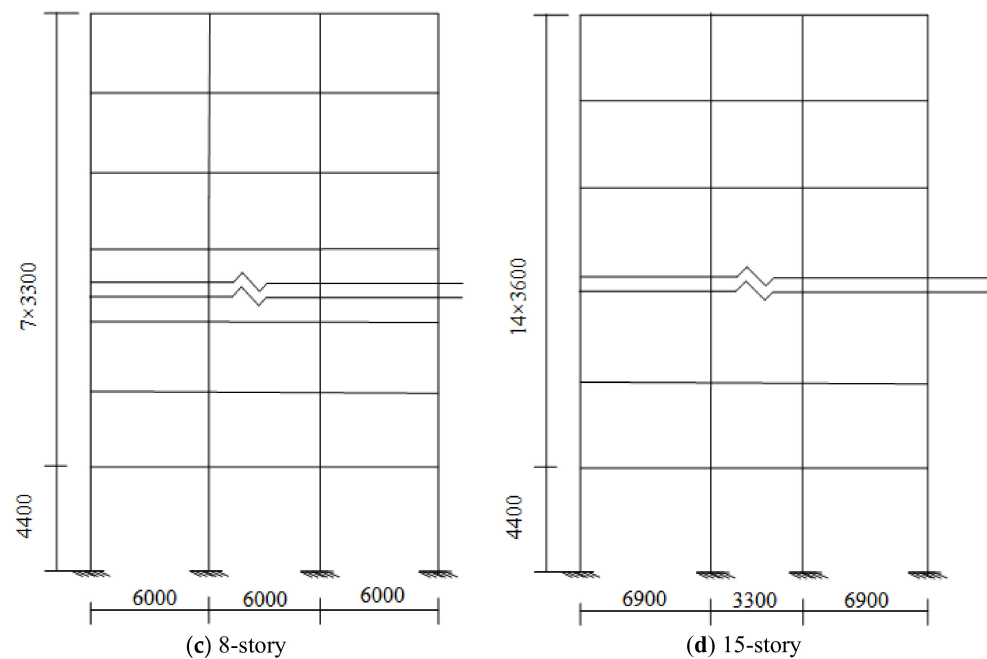


Figure 6. Elevation of four representative reinforced concrete frame structures (unit: mm).

Table 3. Beam section properties of four RC frame buildings.

Structure	Story	Section Size (mm × mm)		Area of Longitudinal Reinforcement (mm ²)/Stirrup (mm ²)	
		Side Column	Middle Column	Side Column	Middle Column
2-story	1–2	600 × 300	600 × 300	1313/φ8@100	1313/φ8@100
5-story	1–4	500 × 250	400 × 250	1008/φ8@100	763/φ8@200
	5	500 × 250	400 × 250	763/φ8@200	603/φ8@200
8-story	1–4	500 × 250	500 × 250	1296/φ8@100	710/φ8@200
	5–6	500 × 250	500 × 250	1015/φ8@100	710/φ8@200
	7–8	500 × 250	500 × 250	710/φ8@100	710/φ8@200
15-story	1–7	600 × 250	450 × 250	1964/φ8@100	935/φ8@100
	8–10	600 × 250	450 × 250	1742/φ8@100	833/φ8@100
	11–12	600 × 250	450 × 250	1520/φ8@100	833/φ8@100
	13–14	600 × 250	450 × 250	1250/φ8@100	833/φ8@100
	15	600 × 250	450 × 250	942/φ8@100	755/φ8@100

The yielding strength f_{yk} of main reinforcement rebars is 400 MPa, and the yielding strength f_{yk} of stirrups is 300 MPa.

Table 4. Column section properties for four RC frame buildings.

Structure	Story	Section Size (mm × mm)		Area of Longitudinal Reinforcement (mm ²)/Stirrup (mm ²)	
		Side Column	Middle Column	Side Column	Middle Column
2-story	1–2	700 × 700	700 × 700	2330/φ8@100	2330/φ8@100
5-story	1–5	500 × 500	500 × 500	2512/φ8@100	2512/φ8@100
8-story	1–5	550 × 550	550 × 550	2733/φ8@100	2733/φ8@100
	6–8	500 × 500	600 × 600	2035/φ8@100	2035/φ8@100
15-story	1–5	650 × 650	650 × 650	4560/φ10@100	4560/φ10@100
	6–10	600 × 600	600 × 600	3807/φ10@100	3807/φ10@100
	11–15	550 × 550	550 × 550	3411/φ8@100	3411/φ8@100

The yielding strength f_{yk} of main reinforcement rebars is 400 MPa, and the yielding strength f_{yk} of stirrups is 300 MPa.

4.2. Selected EDPs

The degree of damage in the structures due to pulse-like ground motions is comprehensively evaluated by selecting several EDPs, as shown in Table 5: (1) MIDR is the maximum

inter-story drift ratio (drift normalized by the story height) over all stories/closely related to local damage, instability, and story collapse; (2) *MFA* is the maximum value of floor absolute acceleration for all stories and indicates the level of non-structural damage; (3) *OSDI* denotes the degree of overall damage in the structure and is determined by the peak displacement and hysteretic energy consumption of the structure.

Table 5. Engineering demand parameters considered in the study.

Num	Notation	Name
1	<i>MIDR</i>	Maximum inter-story drift ratio
2	<i>MFA</i>	Maximum floor acceleration
3	<i>OSDI</i>	Overall structural damage index

5. Prediction and Analysis of EDPs Based on IMs

The capacity of an *IM* for predicting *EDPs* is primarily determined via analyzing the efficiency and sufficiency of the *IM*. In traditional methods [32,35], the numerical values of *IMs* and *EDPs* are typically assumed to have linear or logarithmic distribution, as shown in Equations (1) and (2). The aim of this study is to rank pulse-like ground motions based on their damage potential. To this end, a new data-processing method is proposed. The *IMs* that can be used to efficiently and sufficiently predict *EDPs* are positively correlated with *EDPs*. *IMs* and *EDPs* are separately used to rank ground motions, which are ranked based on *IMs* and *EDPs*, respectively, and the relationship between the two ranking results (R_{IM} and R_{EDP}) is shown in Equation (3). The efficiency and sufficiency of an *IM* is determined by the ability of the *IM* to predict *EDP*.

$$\eta_{D|IM} = b_0 + b_1 IM \quad (1)$$

$$\ln \eta_{D|IM} = b_0 + b_1 \ln IM \quad (2)$$

$$\hat{R}_{EDP} = b_0 + b_1 R_{IM} \quad (3)$$

where b_0 and b_1 are regression coefficients, R_{IM} is the ranking obtained using an *IM*, and R_{EDP} is the ranking obtained using an *EDP*.

5.1. Efficiency of the IMs

Efficiency is an important metric for assessing the quality of a selected *IM*. There are two commonly used statistical parameters that can be used to describe the efficiency of *IMs* [9,40]. The first parameter is the determination coefficient (R^2), as shown in Equation (4). A value of R^2 is closer to one; the efficiency of the *IM* increases with the decrease in the discreteness of *IM* ranking and *EDP* ranking fitting. The second statistical parameter is the standard deviation $\beta_{D|IM}$. The greater the value of $\beta_{D|IM}$, the smaller the dispersion, which means that the regression model is more efficient for characterizing the structural response. Either of the statistical parameters can be used to effectively measure the efficiency of *IMs*. R^2 is used as the criterion in this study.

$$R^2 = \frac{\sum_{k=1}^n (\hat{R}_{EDP} - \bar{R}_{EDP})^2}{\sum_{k=1}^n (R_{EDPk} - \bar{R}_{EDP})^2} \quad (4)$$

where n denotes the number of ground motion data points; \hat{R}_{EDP} denotes the response fitting ranking based on the *IM* ranking; \bar{R}_{EDP} is the average ranking of *EDP*; R_{EDP} is the *EDP* ranking.

The efficiencies of the *IMs* are analyzed based on the structural responses of the four structures, and the calculation results are shown in Figures 7–9. Notably, the uncertainties associated with ground motion and building structure should be considered while analyzing the damage potential of ground motion for building structures. There are no-

table differences between the discreteness of the same *IM* and the same *EDP* for different structures. Furthermore, the discreteness of the same *IM* and different *EDPs* may also be different for the same structure. These results indicate the uncertainties associated with structure. However, in many studies, only similar structures have been analyzed, and the results are inconsistent with the findings of this study [9,26].

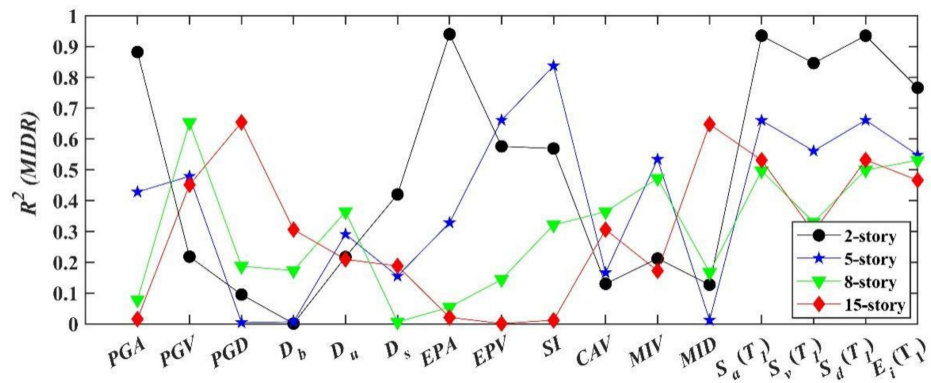


Figure 7. R^2 of *IMs* and *MIDR*, obtained via the cloud analysis of four typical structures subjected to pulse-like ground motions.

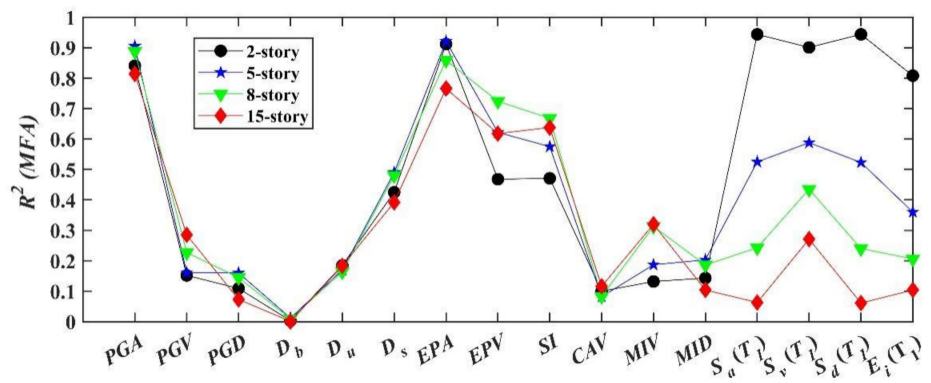


Figure 8. R^2 of *IMs* and *MFA*, obtained via the cloud analysis of four typical structures subjected to pulse-like ground motions.

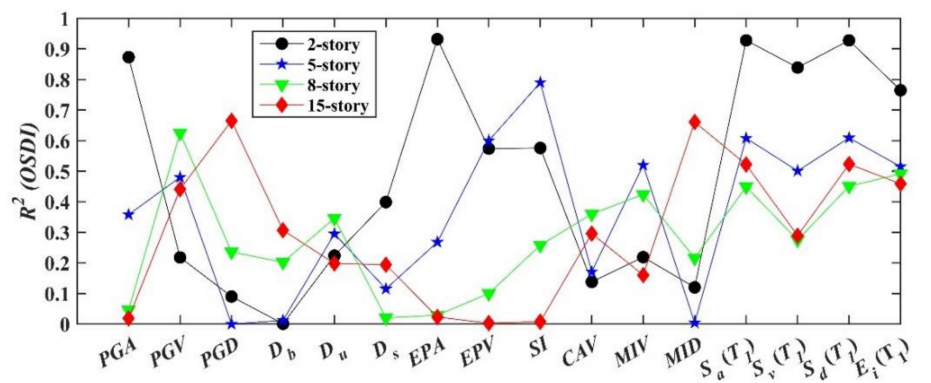


Figure 9. R^2 of *IMs* and *OSDI*, obtained via the cloud analysis of four typical structures subjected to pulse-like ground motions.

In addition, there are significant differences between the R^2 values of different *IMs* and *EDPs* for the same structure; this indicates the uncertainties associated with ground motion. The uncertainties associated with ground motion and building structure are considered in this study for analyzing the ability of *IMs* to predict *EDPs* accurately and to determine

the optimal *IMs* for describing the damage potential of ground motion. Three *IMs* with the largest R^2 for *EDP* prediction are selected for the different structural types and *EDPs*. The results are shown in Table 6. The results indicate that even for the same *EDP*, the most efficient *IMs* are different for different structural types. When *MIDR* is selected as the *EDP*, the most efficient *IMs* are different for different building types: *EPA*, $S_a(T_1)$, and $S_d(T_1)$ are the most efficient *IMs* for two-story buildings; *SI*, *EPV*, and $S_a(T_1)$ are the most efficient *IMs* for five-story buildings; *PGV*, $S_d(T_1)$, and $E(T_1)$ are the most efficient *IMs* for eight-story buildings, and *PGD*, *MID*, and $S_d(T_1)$ are selected as the most efficient *IMs* for 15-story buildings. The *IMs* that can be used to predict *OSDI* and *MIDR* are the same in most cases. Some *IMs* related to acceleration can be used to efficiently characterize *MFA*, such as *PGA*, *EPA*, and $S_a(T_1)$.

Table 6. The most efficient *IMs* for different typical structures.

Models	<i>MIDR</i>	<i>MFA</i>	<i>OSDI</i>
2-story	<i>EPA</i> , $S_a(T_1)$, $S_d(T_1)$	<i>EPA</i> , $S_a(T_1)$, $S_d(T_1)$	<i>EPA</i> , $S_a(T_1)$, $S_d(T_1)$
5-story	<i>SI</i> , <i>EPV</i> , $S_a(T_1)$	<i>PGA</i> , <i>EPA</i> , <i>EPV</i>	<i>SI</i> , $S_a(T_1)$, $S_d(T_1)$
8-story	<i>PGV</i> , $S_d(T_1)$, $E_i(T_1)$	<i>PGA</i> , <i>EPA</i> , <i>EPV</i>	<i>PGV</i> , $S_d(T_1)$, $E(T_1)$
15-story	<i>PGD</i> , <i>MID</i> , $S_d(T_1)$	<i>PGA</i> , <i>EPA</i> , <i>SI</i>	<i>PGD</i> , <i>MID</i> , $S_d(T_1)$

5.2. Sufficiency of the Selected *IMs*

In addition to efficiency, sufficiency is important for assessing the quality of *IMs*. An *IM* is sufficient when the probability distribution of an *EDP* is independent from ground motion characteristics, such as epicenter distance, magnitude, and the ground motion parameter epsilon (ϵ) [41]. Zelaschi et al. [40] obtained *p*-values for the residuals of *EDP* and $\ln \eta_{D|IM}$ with magnitude and epicenter distance of the ground motion when they proved that an *IM* is sufficient. Similar methods [20,29,42] have been used in relevant studies to demonstrate the sufficiency of *IMs*. However, the method proposed by Zelaschi et al. is unreasonable because the calculated *p*-values are closely related to the number of samples, as noted in relevant studies [40,43]. It becomes more difficult to accept the null hypothesis with an increasing number of samples.

The sufficiency of an *IM* can also be verified based on relative entropy, a concept in seismic engineering proposed by Jalayer [27]. In this study, based on the concept of relative entropy, a simple quantitative measure is introduced; it is called the relative sufficiency measure, which is selected as a parameter to measure the relative sufficiency of one *IM* with respect to another. Therefore, the relative sufficiency measure is used to verify the sufficiency of the selected *IMs*. The simplified and approximate formulation of relative sufficiency is shown in Equation (5).

$$I(D|IM_2|IM_1) \approx \frac{1}{n} \sum_{k=1}^n \log_2 \left(\frac{\frac{\beta_{D|IM_1}}{\beta_{D|IM_2}} \varphi \left(\frac{\ln y_k - \ln \eta_{D|IM_2}(IM_{2,K})}{\beta_{D|IM_2}} \right)}{\frac{\beta_{D|IM_2}}{\beta_{D|IM_1}} \varphi \left(\frac{\ln y_k - \ln \eta_{D|IM_1}(IM_{2,K})}{\beta_{D|IM_1}} \right)} \right) \quad (5)$$

where $\beta_{D|IM}$ is the conditional standard deviation, which serves as a quantitative measure for the prediction efficiency of the *IMs*; y_k is the R_{EDP} ; $\ln \eta_{D|IM}$ is the fitting function; n is the number of samples.

The above equation was derived by Jalayer [27] and Ebrahimian [9]. The reference intensity (i.e., IM_1 in Equation (5)) is considered to be $S_a(T_1)$ for the structural response, mainly because $S_a(T_1)$ is a better characterization parameter for the structural response and is extensively used in earthquake engineering. The sufficiency is measured for each candidate *IM* relative to $S_a(T_1)$.

If $I(IM_2|IM_1)$ has a positive value, the candidate *IM* is more sufficient than $S_a(T_1)$. Similarly, if $I(IM_2|IM_1)$ has a negative value, the candidate *IM* is less sufficient than $S_a(T_1)$ for predicting *EDPs*.

The obtained results, as shown in Figures 10–12, indicate that one or more IMs are more sufficient than $S_a(T_1)$ for characterizing the $EDPs$ in most cases. However, when analyzing MFA and $MIDR$ for a two-story structure, all $I(IM_2|IM_1)$ values are not positive, which indicates that $S_a(T_1)$ is the most sufficient among all parameters. Finally, all the most sufficient IMs for characterizing the $EDPs$ are obtained, as shown in Table 7.

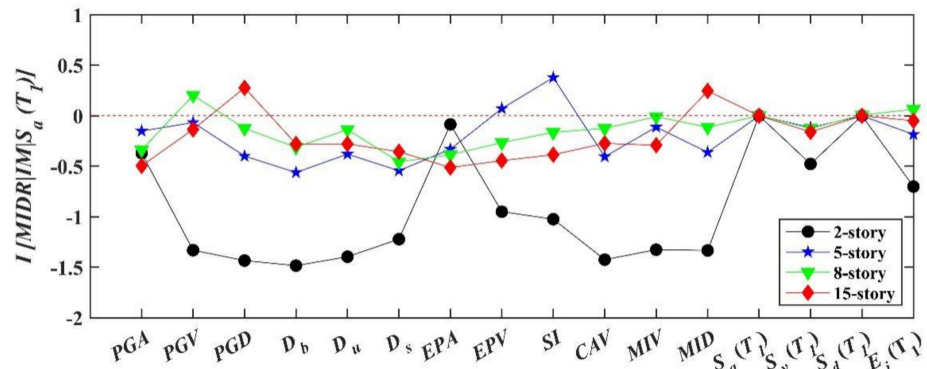


Figure 10. $I(IM_2|IM_1)$ between IMs and $MIDR$, obtained via the cloud analysis of four typical structures subjected to pulse-like ground motions.

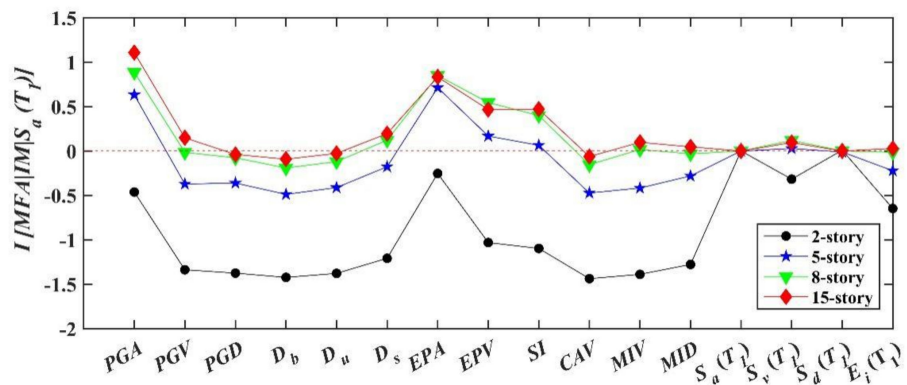


Figure 11. $I(IM_2|IM_1)$ between IMs and MFA , obtained via the cloud analysis of four typical structures subjected to pulse-like ground motions.

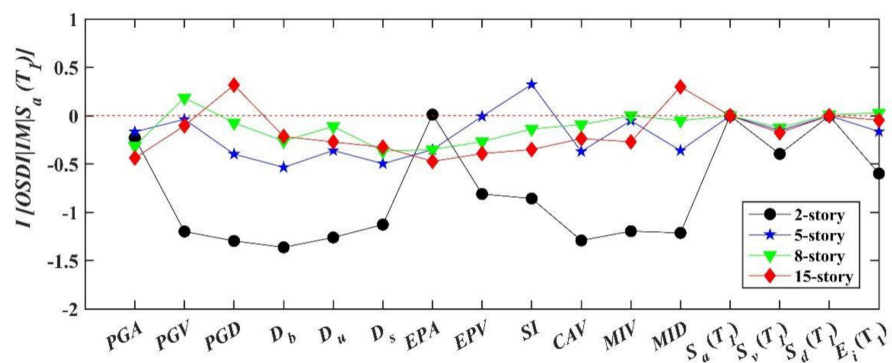


Figure 12. $I(IM_2|IM_1)$ between IMs and $OSDI$, obtained via the cloud analysis of four typical structures subjected to pulse-like ground motions.

Table 7. The most sufficient *IMs* for different structures.

Building Structure	<i>MIDR</i>	<i>MFA</i>	<i>OSDI</i>
2-story	$S_a(T_1)$	$S_a(T_1)$	<i>EPA</i>
5-story	<i>SI, EPV</i>	<i>PGA, EPA, EPV, S_v(T₁)</i>	<i>SI</i>
8-story	<i>PGV, S_d(T₁), E_i(T₁)</i>	<i>PGA, D_s, EPA, EPV, SIMIV, S_v(T₁), S_d(T₁)</i>	<i>PGV, S_d(T₁), E_i(T₁)</i>
15-story	<i>PGD, MID</i>	<i>PGA, D_s, EPA, EPV, SI</i>	<i>PGD, MID, S_d(T₁)</i>

5.3. Comprehensive Analysis of the Selected *IMs*

The efficiency and sufficiency of 16 *IMs* are analyzed to determine the optimal *IMs* for accurately describing the damage potential of ground motions. The ground motion *IMs* that satisfy the requirements of both efficiency and sufficiency are determined by comparing the analysis results for efficiency and sufficiency, as shown in Table 8. For a short-period structure (for example, two-story) and *MFA* as the *EDP*, the acceleration-related *IMs* can be used to efficiently and sufficiently characterize the *EDPs*. For *MIDR* or *OSDI* as the *EDP* and a medium-period structure (for example, eight-story), the velocity-related *IMs* can be used to efficiently and sufficiently characterize the *EDPs*. Finally, the displacement-related *IMs* can be used to efficiently and sufficiently characterize the *MIDR* or *OSDI* for a long-period structure (for example, 15-story).

Table 8. The most efficient and sufficient *IMs* for different buildings.

Building Structure	<i>MIDR</i>	<i>MFA</i>	<i>OSDI</i>
2-story	$S_a(T_1)$	$S_a(T_1)$	<i>EPA</i>
5-story	<i>SI, EPV</i>	<i>PGA, EPA, EPV</i>	<i>SI</i>
8-story	<i>PGV, S_d(T₁), E(T₁)</i>	<i>PGA, EPA, EPV</i>	<i>PGV</i>
15-story	<i>PGD, MID</i>	<i>PGA, EPA</i>	<i>PGD, MID</i>

6. Establishing the Pulse-like Ground Motion Rankings

To describe the destructive capacity of ground motion more accurately and rank the pulse-like ground motions based on the optimal *IMs*, the efficiency and sufficiency of 16 *IMs* are analyzed by four different structures. However, there are two cases based on the number of *IMs*, as shown in Table 8: (1) only one optimal *IM* is obtained, and the pulse-like ground motions are ranked directly based on this *IM*, which is the damage potential ranking result of the pulse-like ground motions; the ranking depicts the ranking in which the ground motions can damage a building structure—the most unfavorable to the most favorable; (2) multiple *IMs* are obtained. However, further analysis is necessary for developing a ranking method in the case of multiple *IMs*.

A novel method is proposed for combining multiple *IMs* into one comprehensive *IM*. The method involves reducing the dimensions of the variables via PCA. Subsequently, the damage potential of pulse-like ground motion is comprehensively evaluated according to the principal component. The results are highly interpretable [44–46].

6.1. Comprehensive *IM* Determination Based on the PCA

The proposed method is a multivariate statistical method that involves dimensional reduction and the transformation of multiple indicators into a few comprehensive indicators, while ensuring minimal loss of data or information. Generally, the comprehensive *IM* generated via transformation is called the principal component, which is a linear combination of original variables. Based on the principal component, the main contradictions can be identified and the collinearity problem between variables can be avoided, and thus the efficiency of the *IM* can be improved.

For example, there are n samples, and each sample contains p variables. A strong correlation exists among these p variables, which is denoted by $X = (x_1, x_2, \dots, x_p)'$ after

standardization. The mathematical model of PCA is shown in Equation (6). \vec{A} is an orthogonal matrix as shown in Equation (7).

$$\begin{cases} y_1 = a_{11}x_1 + a_{12}x_2 + \dots + a_{1p}x_p \\ y_2 = a_{21}x_1 + a_{22}x_2 + \dots + a_{2p}x_p \\ \vdots \\ y_p = a_{p1}x_1 + a_{p2}x_2 + \dots + a_{pp}x_p \end{cases} \quad (6)$$

$$\vec{A} = \begin{bmatrix} a_{11} & a_{12} & \dots & a_{1p} \\ a_{21} & a_{22} & \dots & a_{2p} \\ \vdots & \vdots & \vdots & \vdots \\ a_{p1} & a_{p2} & \dots & a_{pp} \end{bmatrix} \quad (7)$$

where y_1, y_2, \dots, y_p are the principal components. The determination steps of the comprehensive IM based on PCA are as follows.

Step 1: The correlation coefficient matrix is calculated to test whether the variables to be analyzed are suitable for PCA. According to the results in Table 8, there are seven cases for which PCA can be applied: (1) MIDR of 5-story, (2) MFA of 5-story, (3) MIDR of 8-story, (4) MFA of 8-story, (5) MIDR of 15-story, (6) MFA of 15-story, and (7) OSDI of 15-story. The correlation coefficients for IMs under all conditions are depicted in Table 9. Notably, when a high degree of correlation exists between the two IMs under all cases, PCA can be performed.

Table 9. Correlation coefficients for related parameters ($p < 0.05$).

Correlation Coefficients	PGA	PGV	PGD	EPV	$S_d (T_1 = 1.73 \text{ s})$
MID	-	-	0.99	-	-
EPA	0.93	-	-	0.68	-
EPV	0.73	-	-	-	-
SI	-	-	-	0.92	-
$S_d (T_1 = 1.73 \text{ s})$	-	0.73	-	-	-
$E_i (T_1 = 1.73 \text{ s})$	-	0.73	-	-	0.97

Step 2: The characteristic values of the correlation coefficient matrix are calculated under seven cases, and the calculation results are shown in Figure 13.

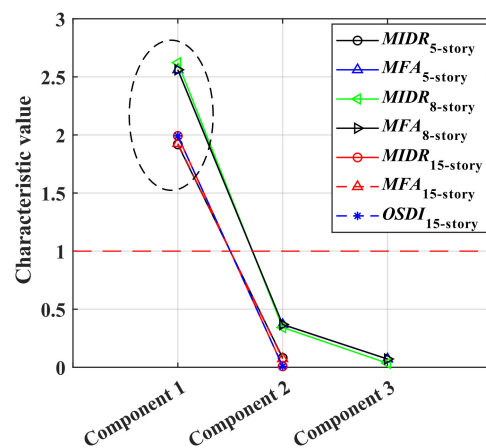


Figure 13. Characteristic values of different components.

Step 3: The number of principal components is determined. There are two situations associated with the determination of the principal component: (1) the cumulative contribution rate of the principal component reaches a certain probability; (2) the characteristic

value is greater than one. The second situation is applied to this study. Based on the characteristic values shown in Figure 13, the number of principal components obtained is one. Therefore, only one principal component f_1 can be used to characterize the damage potential of ground motions.

Step 4: The pulse-like ground motions are ranked based on the principal components. The pulse-like ground motions can be ranked directly based on the first principal component f_1 . Each principal component need not be added to determine the comprehensive score. Table 10 shows the correlation coefficients and component score coefficients between the principal component f_1 and *IMs* under the same case. Note that the principal component is highly correlated with other parameters. The principal component f_1 is calculated as shown in Equation (8).

$$f_1 = c_1IM_1 + c_2IM_2 + \dots + c_nIM_n \quad (8)$$

where c_1, c_2, \dots, c_n are the score coefficients of different *IMs*; n is the number of *IMs*.

Table 10. Correlation coefficients and score coefficients between principal component f_1 and corresponding values.

Building Structure	EDP	IM	Correlation Coefficient ($p < 0.05$)	Score Coefficient
5-story	MIDR	SI	0.98	0.51
		EPV	0.98	0.51
	MFA	PGA	0.96	0.38
		EPA EPV	0.95 0.86	0.37 0.34
8-story	MIDR	PGV	0.87	0.33
		$S_d(T_1)$	0.97	0.37
		$E_i(T_1)$	0.97	0.37
	MFA	PGA EPA EPV	0.96 0.95 0.86	0.38 0.37 0.34
15-story	MIDR	PGD	1.00	0.50
		MID	1.00	0.50
	MFA	PGA EPA	0.98 0.98	0.51 0.51
		OSDI	PGD MID	1.00 1.00

6.2. Ranking of Pulse-like Ground Motions According to Damage Potential

The pulse-like ground motions are ranked according to the selected *IMs* under different cases, as shown in Table 11. If only one *IM* is obtained in certain cases, the pulse-like ground motions can be ranked directly based on that *IM*. In addition, the pulse-like ground motions are ranked according to the principal component f_1 . Furthermore, the ranking results are obtained for the damage potential of pulse-like ground motions for different structures. The ranking results are shown in Appendix A. Due to the large number of ground motion data points, only a few of the ranked ground motion data points are given. The remaining data points are entered in an MS Excel spreadsheet.

Table 11. Ranking of pulse-like ground motions based on optimal *IMs* under different cases.

Type of Structures	Representative Structures	<i>MIDR</i>	<i>MFA</i>	<i>OSDI</i>
Low period	2-story	$S_a(T_1)$	$S_a(T_1)$	<i>EPA</i>
Low and middle period	5-story	$f_{1,(SI,EPV)}$	$f_{1,(PGA,EPA,EPV)}$	<i>SI</i>
Middle and tall period	8-story	$f_{1,(PGV,S_a(T_1),E(T_1))}$	$f_{1,(PGA,EPA,EPV)}$	<i>PGV</i>
Tall period	15-story	$f_{1,(PGD,MID)}$	$f_{1,(PGA,EPA)}$	$f_{1,(PGD,MID)}$

7. Discussion

It is well known that the damage potential of pulse-like ground motions is greater than that of ordinary ground motions. However, previous studies have not yet quantitatively measured the damage potential of pulse-like ground motions for different structures. To solve this challenge, this study proposed a new method to rank pulse-like ground motions based on the damage potential. The method was developed based on 240 pulse-like ground motions and 16 *IMs*. *IMs* were employed to describe the damage potential of ground motions, and *EDPs* were used to characterize the damage state of structures. The relationship between the *IMs* and *EDPs* was analyzed based on four representative RC frame structures to cover a wide range of natural vibration periods, which can better represent the variety of actual structures than the traditional studies with close natural vibration periods. The results of this study indicate that there are notable differences between the discreteness of the *IMs* and the *EDPs* for the RC frame structures with different natural vibration periods. When *MFA* is used as the *EDP*, the acceleration-related *IMs* can be used to efficiently and sufficiently characterize *MFA* for all four structures. When *MIDR* or *OSDI* is used as the *EDP*, the acceleration-related, velocity-related, and displacement-related *IMs* can be used to efficiently and sufficiently characterize *EDP* for short-period structures (e.g., two-story), medium-period structures (e.g., eight-story), and long-period structures (e.g., fifteen-story), respectively.

In addition, the two cases on the selected *IMs* shown in Table 8 indicate that: (1) only one optimal *IM* was obtained for the structures with different natural vibration periods and *EDPs*, respectively; (2) multiple *IMs* were obtained, the PCA method was employed to obtain a comprehensive *IM* to characterize the damage potential of pulse-like ground motions for specific building structures and *EDPs*. The pulse-like ground motions were ranked based on the selected *IM* and the comprehensive *IM* for four structures and three *EDPs*, respectively. The proposed method can quantitatively evaluate the damage potential of pulse-like ground motions for RC frame structures. Note that the proposed ranking method was validated for four representative RC-frame structures, and the feasibility of the method for more types of structures needs further investigation.

8. Conclusions

In this paper, a new method of ranking pulse-like ground motions based on the damage potential was proposed. Four ordinary representative RC frame structures with different natural vibration periods were built, based on which the *IMs* that could predict the damage potential of ground motions for structures were analyzed and obtained. Then, the efficiency and sufficiency of the obtained *IMs* were verified. Finally, the pulse-like ground motions were ranked according to their damage potential. The conclusions of the study are as follows.

- (1) The ground motion *IMs* that can be used to efficiently and sufficiently predict the *EDPs* of different structures are obtained by analyzing the efficiency and sufficiency of 16 *IMs*. First, when the *MFA* is selected as the *EDP*, the acceleration-related *IMs* can efficiently determine the *EDP*. Second, when *MIDR* or *OSDI* is selected as the *EDP*, the acceleration-related, velocity-related, and displacement-related *IMs* can be used to effectively determine the *EDPs* of short-period structures (for example, two-story), medium-period structures (for example, eight-story), and long-period structures (for example, 15-story), respectively.

- (2) The PCA method is used to reduce the variable dimensions of the *IMs* selected under seven conditions, and the principal component f_1 is selected as the comprehensive *IM* that can reflect the damage potential of multiple *IMs*.
- (3) The pulse-like ground motions are ranked based on the selected *IMs* and the comprehensive *IM* under different cases. Finally, the damage-potential-based ranking of the pulse-like ground motions is completed.

The damage potential ranking method proposed in this study can quantitatively evaluate the damage potential of pulse-like ground motions. The ranking results of 240 pulse-like ground motions provide a database for selecting ground motions in seismic design of RC-frame structures.

Author Contributions: Conceptualization, Q.L. and J.H.; methodology, L.X. (Lili Xie); software, Q.L.; validation, Q.L., J.H., L.X. (Lili Xie) and L.X. (Longjun Xu); formal analysis, L.X. (Longjun Xu) and S.L.; investigation, S.L.; resources, S.L.; data curation, Q.L.; writing—original draft preparation, Q.L.; writing—review and editing, J.H.; visualization, J.H.; supervision, L.X. (Lili Xie); project administration, L.X. (Longjun Xu); funding acquisition, L.X. (Longjun Xu). All authors have read and agreed to the published version of the manuscript.

Funding: This research was funded by the National Natural Science Foundation of China, grant number [U2139207; U1939210]. Additionally, the APC was funded by [U2139207].

Institutional Review Board Statement: Not applicable.

Informed Consent Statement: Not applicable.

Data Availability Statement: Not applicable.

Acknowledgments: The work is supported by the National Natural Science Foundation of China (Grant No. U2139207; U1939210). The support is gratefully acknowledged. The authors would also like to thank the NGA-West2 database for providing the strong ground motion data.

Conflicts of Interest: The authors declare no conflict of interest.

Appendix A

Table A1. Damage potential ranking of pulse-like ground motions.

Ranking Number	2-Story		5-Story			8-Story			15-Story	
	MIDR and MFA	OSDI	MIDR	MFA	OSDI	MIDR	MFA	OSDI	MIDR and OSDI	MFA
1	GBZ000	GBZ000	H-E03140	H-E05140	SKR090	SKR090	H-E05140	TCU059-N	TCU059-N	H-E05140
6	PUL194	PUL194	SCE288	DZC270	SCE288	YPT330	DZC270	TCU057-W	TCU057-W	DZC270
11	H-E03230	H-E03230	WPI046	PAR-T	WPI046	TCU060-W	PAR-T	SCR090	TCU026-W	H-E03230
16	H-E11230	H-E11230	LDM334	TCU068-N	H-E10320	TCU115-W	TCU068-N	A-BIR180	SHI000	SCR090
21	DZC180	DZC180	CPM000	H-E06140	WPI316	DZC270	H-E06140	SCE288	TCU046-W	H-ECC002
26	TAK090	TAK090	TCU060-W	TCU057-W	TCU059-W	H-E11230	TCU057-W	TCU115-W	TCU065-W	TCU057-W
31	H-E06140	H-E06140	ERZ-NS	CPM000	ERZ-NS	ERZ-NS	CPM000	CHY002-N	TCU056-N	SKR090
36	LCN000	LCN000	MUL279	D-TSM270	CNP196	TCU116-W	D-TSM270	SHI000	TCU029-N	WPI316
41	ORR090	ORR090	WVC000	SCE018	WVC000	WPI316	SCE018	CPM000	TCU076-N	LDM334
46	A-OR2010	A-OR2010	ORR090	TCU128-W	H-E04230	LDM334	TCU128-W	H-E11230	CHY101-W	SCE018
51	CPM000	CPM000	H-HVP225	SPV270	D-TSM270	H-HVP315	SPV270	TCU103-W	TCU045-W	TCU111-W
56	LDM334	LDM334	D-TSM360	DZC180	STN110	H-ECC002	DZC180	TCU057-N	CHY029-N	SCS142
61	GOF090	GOF090	TCU120-W	RIO270	TCU063-N	ORR090	RIO270	TCU063-N	TCU047-N	TCU059-W
66	HSP000	HSP000	40I07EW	MUL279	H-BRA315	A-OR2010	MUL279	WVC000	TCU094-W	UNI005
71	STG000	STG000	A-ZAK360	MVH135	H-E08140	SPV270	MVH135	TCU087-W	TCU100-W	TCU038-W
76	40E01EW	40E01EW	YER270	NAS270	H-BRA225	40I07EW	NAS270	TCU049-W	TCU064-N	TCU068-W
81	TCU059-N	TCU059-N	MU2035	WWT180	LOS000	TRI090	WWT180	TCU096-W	ILA037-N	H-BRA225
86	CPM090	CPM090	H-AGR273	H-HVP225	TCU095-N	TCU060-N	H-HVP225	A-OR2010	TCU070-N	ERZ-NS
91	40I01EW	40I01EW	CPM090	D-PVY045	DZC180	TCU026-W	D-PVY045	H-BRA315	TCU098-N	D-PVY045
96	UNI005	UNI005	TCU055-N	TCU057-N	TCU068-N	TCU103-W	TCU057-N	H-E06140	HSP000	H-E10050
101	SCS052	SCS052	A-BAG270	TAB-LN	CYC285	TCU076-N	TAB-LN	TCU095-N	TCU095-W	ARC090
106	WWT270	WWT270	40E01EW	WVC270	D-OLC270	TCU136-E	WVC270	TCU026-W	CHY006-E	WVC270
111	TCU115-W	TCU115-W	TCU052-W	TCU116-W	NPS210	40E01EW	TCU116-W	TCU068-N	YPT330	BOL090
116	TCU045-N	TCU045-N	SPG360	40E01EW	G01090	TCU040-N	40E01EW	TCU039-N	A02043	A-ZAK360
121	TCU031-W	TCU031-W	A02043	TCU040-N	H-QKP085	TCU045-N	TCU040-N	JEN022	H-AGR273	TCU040-N
126	TCU049-N	TCU049-N	MUL009	TAZ000	TCU048-N	TCU049-W	TAZ000	TCU076-N	A02133	TCU117-W

Table A1. Cont.

Ranking Number	2-Story		5-Story		8-Story			15-Story		
	MIDR and MFA	OSDI	MIDR	MFA	OSDI	MIDR	MFA	OSDI	MIDR and OSDI	MFA
131	STG090	STG090	TCU049-N	STG000	GAZ000	MU2035	STG000	MU2035	TCU064-W	STG000
136	TCU117-W	TCU117-W	H-AGR003	TCU105-N	TCU109-W	G01090	TCU105-N	PAC265	TCU075-W	KJM090
141	TCU046-W	TCU046-W	TCU104-N	H-E11140	GOF090	H-BRA225	H-E11140	TCU051-W	40I01EW	H-BRA315
146	S2330	S2330	TCU026-W	TCU100-N	TCU128-N	C02065	TCU042-W	TCU042-W	H-HVP315	TCU045-N
151	KJM090	KJM090	TAB-TR	HVR240	ARC090	TCU039-W	HVR240	TCU076-W	WPI316	HVR240
156	PAC175	PAC175	TCU034-W	TCU098-N	TCU018-W	TCU017-W	TCU098-N	H-E06230	H-E03140	TAZ090
161	A02133	A02133	FOR000	A02133	TCU046-W	STG000	A02133	LGF000	CHY002-N	H-QKP085
166	G06090	G06090	TAZ000	TCU055-N	H-AEP045	TCU083-W	TCU055-N	TCU036-N	GOF090	TAB-TR
171	TCU083-W	TCU083-W	TCU031-W	TCU104-N	TCU105-W	TCU105-W	TCU104-N	TCU070-N	NAS270	TCU095-N
176	TCU048-N	TCU048-N	TCU050-N	TCU039-N	SCS052	TCU017-N	TCU039-N	DZC180	PAR-L	NSY-N
181	TCU050-W	TCU050-W	STG000	TCU103-W	TCU003-W	CHY101-N	TCU103-W	TCU048-N	TAK000	TCU109-W
186	PRS090	PRS090	TCU067-W	H-FRN044	PAC175	D-OLC270	H-FRN044	KJM090	PRS090	TCU029-N
191	TCU104-W	TCU104-W	TCU015-W	TCU087-W	TCU050-W	MUL009	TCU087-W	40I07EW	CNP196	H-FRN044
196	TCU064-W	TCU064-W	TCU076-N	TCU015-W	TCU104-W	H-QKP085	TCU015-W	TCU067-N	G06230	TCU015-W
201	TCU105-W	TCU105-W	TCU083-W	TCU010-W	TCU083-W	TCU064-W	TCU010-W	TCU053-N	MU2035	TCU104-W
206	CHY080-N	CHY080-N	TCU029-N	TCU083-W	TCU051-W	TCU036-N	TCU083-W	G06090	CYC195	TCU065-W
211	TCU029-W	TCU029-W	TCU047-N	TCU096-W	CHY101-N	TCU089-N	TCU096-W	TCU095-W	GAZ000	TCU095-W
216	JEN292	JEN292	TCU098-W	TCU064-W	TCU089-N	PAC175	TCU064-W	H-QKP085	H-BRA225	TCU064-W
221	GAZ090	GAZ090	S2330	TCU076-N	TCU075-W	CHY029-N	TCU076-N	H-FRN044	H-E08140	TCU053-W
226	TCU-E	TCU-E	TCU029-W	CHY080-W	TCU064-N	CHY028-W	CHY080-W	PAC175	CPM090	CHY080-W
231	CHY080-W	CHY080-W	TCU087-N	CHY029-N	TCU-E	H-ECC092	CHY029-N	CHY029-N	H-E07140	CHY029-N
236	TCU067-N	TCU067-N	TCU067-N	TCU067-N	TCU067-N	40I01EW	TCU067-N	TCU067-W	LDM064	TCU067-N

Note: 1. Due to the large number of ground motion records, only a part of the ground motion records are given. Others are given in electronic form. 2. For the same structure, when the IMs representing the two structural response indexes are the same, a ranking result is used.

References

- Kalkan, E.; Kunnath, S.K. Effects of fling step and forward directivity on seismic response of buildings. *Earthq. Spectra* **2006**, *22*, 367–390. [[CrossRef](#)]
- Sehhati, R.; Rodriguezm, M.A.; Elgawady, M.; Cofer, W.F. Effects of near-fault ground motions and equivalent pulses on multi-story structures. *Eng. Struct.* **2011**, *33*, 767–779. [[CrossRef](#)]
- Champion, C.; Liel, A. The effect of near-fault directivity on building seismic collapse risk. *Earthq. Eng. Struct. Dynam.* **2012**, *41*, 1391–1409. [[CrossRef](#)]
- Wen, W.P.; Zhai, C.H.; Li, S.; Chang, Z.W.; Xie, L.L. Constant damage inelastic displacement for the near-fault pulse-like ground motions. *Eng. Struct.* **2014**, *59*, 599–607. [[CrossRef](#)]
- Bazzurro, P. Probabilistic Seismic Demand Analysis. Ph.D. Thesis, Department of Civil Engineering, Stanford University, Stanford, CA, USA, 1998.
- FEMA-355; State of the Art Report on Systems Performance of Steel Moment Frames Subject to Earthquake Ground Shaking. SAC Joint Venture: Sacramento, CA, USA, 2000.
- Moehle, J.; Deierlein, G.G. A framework methodology for performance-based earthquake engineering. In Proceedings of the 13th World Conference on Earthquake Engineering, Vancouver, BC, Canada, 1–6 August 2004.
- Kostinakis, K.; Fontara, I.K.; Athanatopoulou, A.M. Scalar Structure-Specific Ground Motion Intensity Measures for Assessing the Seismic Performance of Structures: A Review. *J. Earthq. Eng.* **2018**, *22*, 630–665. [[CrossRef](#)]
- Ebrahimian, H.; Jalayer, F.; Lucchini, A.; Mollaioli, F.; Manfredi, G. Preliminary ranking of alternative scalar and vector intensity measures of ground shaking. *Bull. Earthq. Eng.* **2015**, *13*, 2805–2840. [[CrossRef](#)]
- Iervolino, I.; Chioccarelli, E.; Baltzopoulos, G. Inelastic displacement ratio of near-source pulse-like ground motions. *Earthq. Eng. Struct. Dyn.* **2012**, *41*, 2351–2357. [[CrossRef](#)]
- Yazdani, A.; Yazdannejad, K. Estimation of the seismic demand model for different damage levels. *Eng. Struct.* **2019**, *194*, 183–195. [[CrossRef](#)]
- Kramer, S.L. *Geotechnical Earthquake Engineering*; Prentice Hall: Englewood Cliffs, NJ, USA, 1996.
- Shome, N.; Cornell, C.A.; Bazzurro, P.; Carballo, J.E. Earthquakes, records and nonlinear responses. *Earthq. Spectra* **1998**, *14*, 469–500. [[CrossRef](#)]
- Gardoni, P.; Mosalam, K.M.; Kiureghian, A.D. Probabilistic seismic demand models and fragility estimates for R.C. bridges. *J. Earthq. Eng.* **2003**, *7*, 79–106. [[CrossRef](#)]
- Jalayer, F. Direct Probabilistic Seismic Analysis: Implementing Nonlinear Dynamic Assessments. Ph.D. Thesis, Department of civil and Environmental Engineering, Stanford University, Stanford, CA, USA, 2003.
- Baker, J.W.; Cornell, C.A. A vector-valued ground motion intensity measure consisting of spectral acceleration and epsilon. *Earthq. Eng. Struct. Dyn.* **2005**, *34*, 1193–1217. [[CrossRef](#)]
- Ramamoorthy, S.K. Seismic Fragility Estimates for Reinforced Concrete Framed Buildings. Ph.D. Thesis, Texas A&M University, College Station, TX, USA, 2006.

18. Tothong, P.; Cornell, C.A. Structural performance assessment under near-source pulse-like ground motions using advanced ground motion intensity measures. *Earthq. Eng. Struct. Dyn.* **2008**, *37*, 1013–1037. [[CrossRef](#)]
19. Jeong, S.H.; Mwafy, A.M.; Elnashai, A.S. Probabilistic seismic performance assessment of code-compliant multi-story RC buildings engineering structures. *Eng. Struct.* **2012**, *34*, 527–537. [[CrossRef](#)]
20. Zhang, Y.; He, Z. Appropriate ground motion intensity measures for estimating the earthquake demand of floor acceleration-sensitive elements in super high-rise buildings. *Struct. Infrastruct. Eng.* **2018**, *15*, 1–17. [[CrossRef](#)]
21. Guan, M.; Du, H.; Cui, J.; Zeng, Q.; Jiang, H. Optimal ground motion intensity measure for long-period structures. *Meas. Sci. Technol.* **2015**, *26*, 105001. [[CrossRef](#)]
22. Tothong, P.; Luco, N. Probabilistic seismic demand analysis using advanced ground motion intensity measures. *Earthq. Eng. Struct. Dyn.* **2007**, *36*, 1837–1860. [[CrossRef](#)]
23. Zengin, E.; Abrahamson, N.A. A vector-valued intensity measure for near-fault ground motions. *Earthq. Eng. Struct. Dyn.* **2020**, *49*, 716–734. [[CrossRef](#)]
24. Jamshidiha, H.R.; Yakhchalian, M. New vector-valued intensity measure for predicting the collapse capacity of steel moment resisting frames with viscous dampers. *Soil. Dyn. Earthq. Eng.* **2019**, *125*, 105625. [[CrossRef](#)]
25. Luco, N.; Cornell, C.A. Structure-specific scalar intensity measures for near-source and ordinary earthquake ground motions. *Earthq. Spectra* **2007**, *23*, 357–392. [[CrossRef](#)]
26. Dávalos, H.; Miranda, E. Filtered incremental velocity: A novel approach in intensity measures for seismic collapse estimation. *Earthq. Eng. Struct. Dyn.* **2019**, *48*, 1384–1405. [[CrossRef](#)]
27. Jalayer, F.; Beck, J.L.; Zareian, F. Analyzing the sufficiency of alternative scalar and vector intensity measures of ground shaking based on information theory. *J. Eng. Mech.* **2012**, *138*, 307–316. [[CrossRef](#)]
28. Palanci, M.; Senel, S.M. Correlation of earthquake intensity measures and spectral displacement demands in building type structures. *Soil. Dyn. Earthq. Eng.* **2019**, *121*, 306–326. [[CrossRef](#)]
29. Yakhchalian, M.; Ghodrati, A.G. A vector intensity measure to reliably predict maximum drift in low- to mid-rise buildings. *Proc. Inst. Civ. Eng. Struct. Build.* **2019**, *172*, 42–54. [[CrossRef](#)]
30. Dávalos, H.; Miranda, E. Robustness evaluation of fiv3 using near-fault pulse-like ground motions. *Eng. Struct.* **2021**, *230*, 111694. [[CrossRef](#)]
31. Papatirou, A.; Athanatopoulou, A. Seismic Intensity Measures Optimized for Low-rise Reinforced Concrete Frame Structures. *J. Earthq. Eng.* **2021**, *25*, 1–39. [[CrossRef](#)]
32. Zhai, C.H.; Li, C.H.; Kunnath, S. An efficient algorithm for identifying pulse-like ground motions based on significant velocity half-cycles. *Earthq. Eng. Struct. Dyn.* **2018**, *47*, 757–777. [[CrossRef](#)]
33. Chen, X.Y.; Wang, D.S.; Zhang, R. Identification of Pulse Periods in Near-Fault Ground Motions Using the HHT Method. *Bull. Seismol. Soc. Am.* **2019**, *109*, 201–212. [[CrossRef](#)]
34. Ye, L.P.; Ma, Q.L.; Miao, Z.W.; Guan, H.; Yan, Z.G. Numerical and comparative study of earthquake intensity indices in seismic analysis. *Struct. Des. Tall. Spec.* **2013**, *22*, 362–381. [[CrossRef](#)]
35. Zhai, C.H.; Chang, Z.W.; Li, S.; Xie, L.L. Selection of the most unfavorable real ground motions for low- and mid-rise RC frame structures. *J. Earthq. Eng.* **2013**, *17*, 1233–1251. [[CrossRef](#)]
36. Li, S.; He, Y.; Wei, Y. Truncation Method of Ground Motion Records Based on the Equivalence of Structural Maximum Displacement Responses. *J. Earthq. Eng.* **2021**, *5*, 1–22. [[CrossRef](#)]
37. Reinhorn, A.M.; Roh, H.; Sivaselvan, M.; Kunnath, S.K.; Valles, R.E.; Madan, A.; Li, C.; Lobo, R.; Park, Y.J. *IDARC-2D Version 7: A Program for Inelastic Damage Analysis of Structures*; State University of New York: Buffalo, NY, USA, 2010.
38. Ibarra, L.F.; Medina, R.A.; Krawinkler, H. Hysteretic models that incorporate strength and stiffness deterioration. *Earthq. Eng. Struct. Dyn.* **2005**, *34*, 1489–1511. [[CrossRef](#)]
39. Ibarra, L.F.; Krawinkler, H. Variance of collapse capacity of SDOF systems under earthquake excitations. *Earthq. Eng. Struct. Dyn.* **2011**, *40*, 1299–1314. [[CrossRef](#)]
40. Zelaschi, C.; Ricardo, M.; Rui, P. Critical Assessment of Intensity Measures for Seismic Response of Italian RC Bridge Portfolios. *J. Earthq. Eng.* **2019**, *23*, 980–1000. [[CrossRef](#)]
41. Baker, J.; Cornell, C.A. Spectral shape, epsilon and record selection. *Earthq. Eng. Struct. Dyn.* **2006**, *35*, 1077–1095. [[CrossRef](#)]
42. Yang, G.; Xie, L.; Li, A.Q. Ground motion intensity measures for seismically isolated RC tall buildings. *Soil. Dyn. Earthq. Eng.* **2019**, *125*, 105727. [[CrossRef](#)]
43. Goodman, S. A dirty dozen: Twelve p-value misconceptions. *Seminars in Hematology. WB Saunders.* **2008**, *45*, 135–140.
44. Kim, K.I.; Jung, K.; Hang, J.K. Face recognition using kernel principal component analysis. *IEEE. Signal. Proc. Lett.* **2002**, *9*, 40–42.
45. Sayed, A.A. Principal component analysis within nuclear structure. *Nucl. Phys. A* **2015**, *933*, 154–164. [[CrossRef](#)]
46. Ana, F.N.; Filipe, M.; Diego, Z.S. Deep Learning Enhanced Principal Component Analysis for Structural Health Monitoring. *Struct. Health Monit.* **2022**, *10*, 14759217211041684.